Data supplement for Chung et al., Synaptic Variability and Cortical Gamma Oscillation Power in Schizophrenia. Am J Psychiatry (doi: 10.1176/appi.ajp.2021.21080798)

Supplemental Methods

Immunohistochemistry

As previously described (1), paraformaldehyde-fixed cryostat sections (40 μm) containing DLPFC area 9 were pretreated for antigen retrieval (0.01 M sodium citrate for 75 min at 80 °C) and incubated for 72 hours at 4 °C in the following primary antibodies: PV (mouse, 1:1000; Swant), CR (goat, 1:1000; Swant), PSD95 (rabbit, 1:250; Cell signaling), and VGlut1 (guinea pig, 1:250; Millipore). Sections were washed in PBS and then incubated for 24 hours at 4 °C in the secondary antibodies (donkey) conjugated to Alexa 488 (anti-mouse, 1:500; Invitrogen), 568 (anti-rabbit, 1:500; Invitrogen), 647 (anti-guinea pig, 1:500; Millipore) or biotin (anti-goat, 1:200; Fitzgerald). Sections were then incubated for 24 hours at 4 °C in streptavidin 405 (1:200; Invitrogen). Sections were then mounted in Prolong Gold Antifade reagent (Life Technologies) and stored at 4 °C until imaging.

Image acquisition and post-image processing

Images containing DLPFC sections were acquired on an Olympus IX81 microscope with a spinning disk confocal unit and a Hamamatsu EM-CCD digital camera at 60x magnification. Ten image stacks (512 X 512 pixel; 0.25 μm z step) in layer 2 or 4, defined as 10-20% or 50-60% of the pia-to-white matter distance, respectively, were randomly sampled. Each fluorescent channel was deconvolved using the Autoquant's Blind Deconvolution algorithm to improve image contrast by reducing

out-of-focus fluorescence. Edges of PV+ or CR+ cell bodies were segmented by the MATLAB edge function using the Canny edge detector operator. The edges of segmented objects were closed, filled and size gated (>80 µm^3) to limit the boundaries of cell bodies. All cell body masks were manually cleaned for final analyses. To segment VGlut1+ and PSD95+ puncta, a custom channel was made for each deconvolved channel of VGlut1 or PSD95 by calculating a difference of Gaussians using sigma values of 0.7 and 2. The Ridler-Calvard threshold value was then applied to the fluorescence intensity histogram of VGlut1+ or PSD95+ labeling and all pixels were assigned ta binary value of 1 or 0 according to whether they were above or below, respectively, the threshold value. The resulting binary objects were defined as VGlut1+ or PSD95+ masks if they fell in the range of defined puncta size (0.06-0.7 µm^3). Multiple iteration of binary masking process was then performed with the threshold level incrementally increasing for each iteration of masking until it reached the highest intensity value. The resulting masks from each iteration were combined to represent the total population of VGlut1+ or PSD95+ puncta. Excitatory inputs to PVIs were defined as overlapping VGlut1+ puncta and PSD95+ puncta within PV+ cell bodies (**Figure S1**).

Computational model network of excitatory and fast-spiking inhibitory cells

We previously built a pyramidal interneuron gamma (PING) model network that generates robust oscillatory activity at gamma frequency and can be used to simulate how gamma power is regulated by various properties of excitatory and inhibitory synapses onto pyramidal or PV neurons (2, 3). In this study, we implement a PING model network that consists of 80 regular-spiking excitatory cells (RSEs) and 20 fast-spiking inhibitory cells (FSIs) to reflect the proportion of inhibitory neurons in primate

prefrontal cortex (4, 5). The RSEs and FSIs in the network are connected to every other

cell (all-to-all connection) via AMPA, NMDA and GABA synapses (**Figure 1A**), so that

the probability of connectivity from RSE-to-RSE ($Conn_{ee}$), RSE-to-FSI ($Conn_{ei}$), FSI-to-

RSE ($Conn_{ie}$) and FSI-to-FSI ($Conn_{ii}$) was set to 1 for all experiments except for **Figure**

5A in which $Conn_{ei}$ was varied from 1 to 0.

Dynamics of the membrane potential (V) of each RSE or FSI over time (t) is

described by the following equations of a quadratic integrate-and-fire neuron (6):

$$C\frac{dV}{dt} = I_{appl} + g_l\frac{(V - V_l)(V - V_T)}{V_T - V_l} - z(V - V_K) - I_{syn} + \sigma N$$

$$\frac{dz}{dt} = -az$$

$$\text{if } V(t) \geq V_{spike}, \text{ then } V(t) \leftarrow V_R$$

In this model, cells spike when their $V(t)$ reaches the spike voltage (V_{spike}).

Once cells spike, their $V(t)$ returns to the reset voltage (V_R). The regular spiking

property of RSE (**Figure 1B, left panel**) was modeled using the following parameters:

V_{spike} = 20 mV, V_R = -70 mV, membrane capacitance (C) = 1 µF/cm^2, leak maximum

conductance (g_l) = 0.1 mS/cm^2, leak equilibrium potential (V_l) = -65 mV and threshold

potential (V_T) = -50 mV. Spike-frequency adaptation in RSE is represented by a

potassium conductance (z) with a decay time constant (a = 0.0125 ms) and an adapting

current potential (V_K = -85 mV); z is incremented by d = 0.05 each time RSEs spike.

The fast-spiking property of FSIs (**Figure 1B, right panel**) was modeled using the same

parameters except for V_R = -60 mV, g_l = 0.2 mS/cm^2 and d = 0 which reflects the

absence of spike-frequency adaptation in PV neurons. A small amount of Gaussian noise (σN; σ = 0.05) was added to all cells. All parameters were set so that at rest RSEs and FSIs have membrane time constants of 20 ms and 10 ms, respectively. Network activity is initiated by a random tonic current (I_{appl}, 3-5 µA/cm²) that is applied to RSEs only. Each RSE or FSI receives synaptic currents (I_{syn}) from their presynaptic cells and the summation of I_{syn} is divided by the number of presynaptic cells.

The synaptic currents are described by the following equation:

$$I_{syn} = (g_e s_e + g_n s_n)(V - V_{ex}) + g_i s_i (V - V_{in})$$

where AMPA and NMDA equilibrium potential (V_{ex}) = 0 mV and GABA equilibrium potential (V_{in}) = -70 mV. The dynamics of synaptic gating (the fraction of open channels) for AMPA (s_e), NMDA (s_n) and GABA synapse (s_i) are described by the following equations:

$$\frac{ds_e}{dt} = -\frac{s_e}{\tau_e}$$

$$\frac{ds_n}{dt} = a_n s_e (1 - s_n) - \frac{s_n}{\tau_n}$$

$$\frac{ds_i}{dt} = -\frac{s_i}{\tau_i}$$

Here, each time a presynaptic RSE or FSI spikes, the s_e or s_i, respectively, of a postsynaptic cell is incremented by 1. The NMDA synaptic gating does not account for

magnesium block as previously described (2, 7). The mean AMPA conductance from RSE-to-FSI ($\bar{g}_{ei}$) and the mean GABA conductance from FSI-to-RSE ($\bar{g}_{ie}$) were varied as stated in each experimental condition while the mean AMPA conductance from RSE-to-RSE ($\bar{g}_{ee}$) and the mean GABA conductance from FSI-to-FSI ($\bar{g}_{ii}$) were set to 1 in all experimental conditions. The mean NMDA conductance from RSE-to-RSE ($\bar{g}_{ne}$) or RSE-to-FSI cells ($\bar{g}_{ni}$) was set to 0.25 or 0.1 in all experimental conditions, respectively, to reflect the AMPA-to-NMDA ratios observed in cortical pyramidal and PV neurons (2). The decay time constants for AMPA (s_e), NMDA (s_n) and GABA (s_i) conductances were set to 2 ms, 80 ms and 7 ms, respectively. The simulation lasted t = 2 s with a step size of dt = 0.5 ms. Power spectral density was taken on the total s_e of RSEs, which reflects population network activity (**Figure 1C, D**) (3). Peak gamma band power for each experimental condition was computed as an average over 200 trials. All simulations were performed in MATLAB (MathWorks, Natick, MA).

FIGURE S1. Sampling VGlut1 and PSD95 levels within excitatory inputs to PVIs in human PFC layer 4
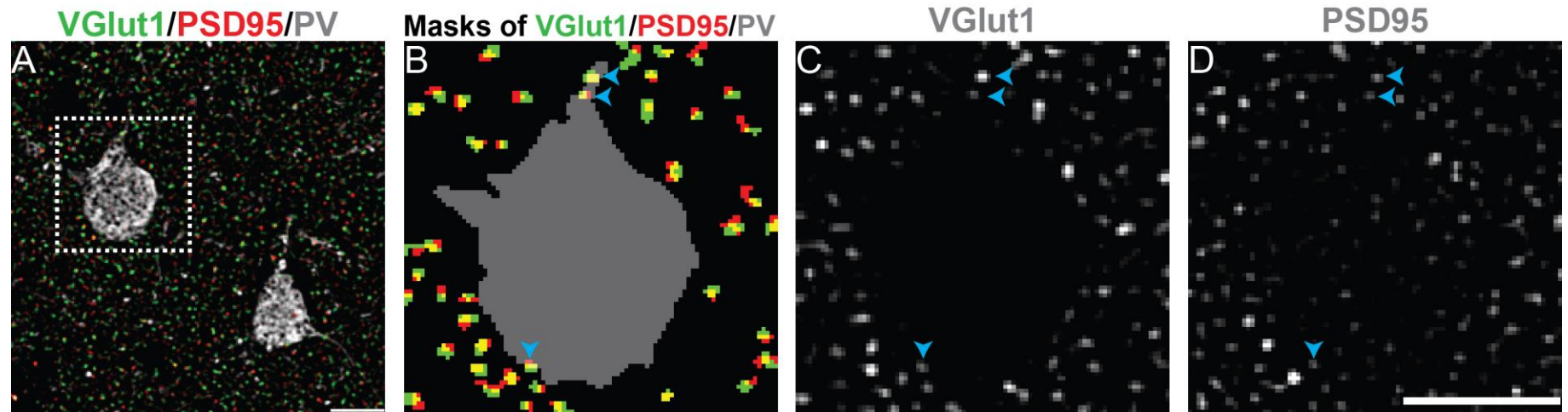

(A) Representative deconvolved image of a human PFC section labeled with antibodies against VGlut1, PSD95 and PV. (B) Combined mask images of VGlut1+ puncta, PSD95+ puncta and PV+ cell body from the boxed area in panel A. Only overlapping VGlut1+ and PSD95+ puncta are displayed. Excitatory inputs to PVIs were defined by the overlapping VGlut1+ and PSD95+ puncta within a PV+ cell body, as indicated by blue arrowheads. (C, D) Gray scale images of VGlut1 (C) and PSD95 (D) immunoreactivity. Levels of VGlut1 and PSD95 immunoreactivity within excitatory inputs to a PVI, indicated by blue arrowheads, were obtained to estimate excitatory synaptic strength onto that PVI. Scale bars=10 μm.

FIGURE S2. Lack of effect from disease-associated comorbid factors on greater synaptic variability across PVIs
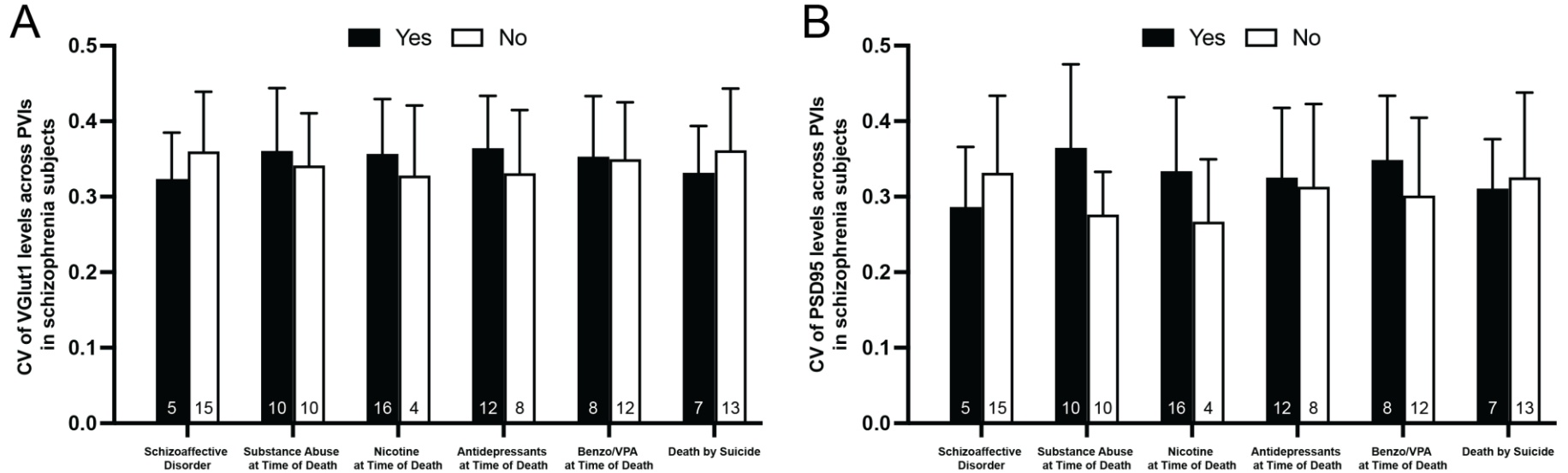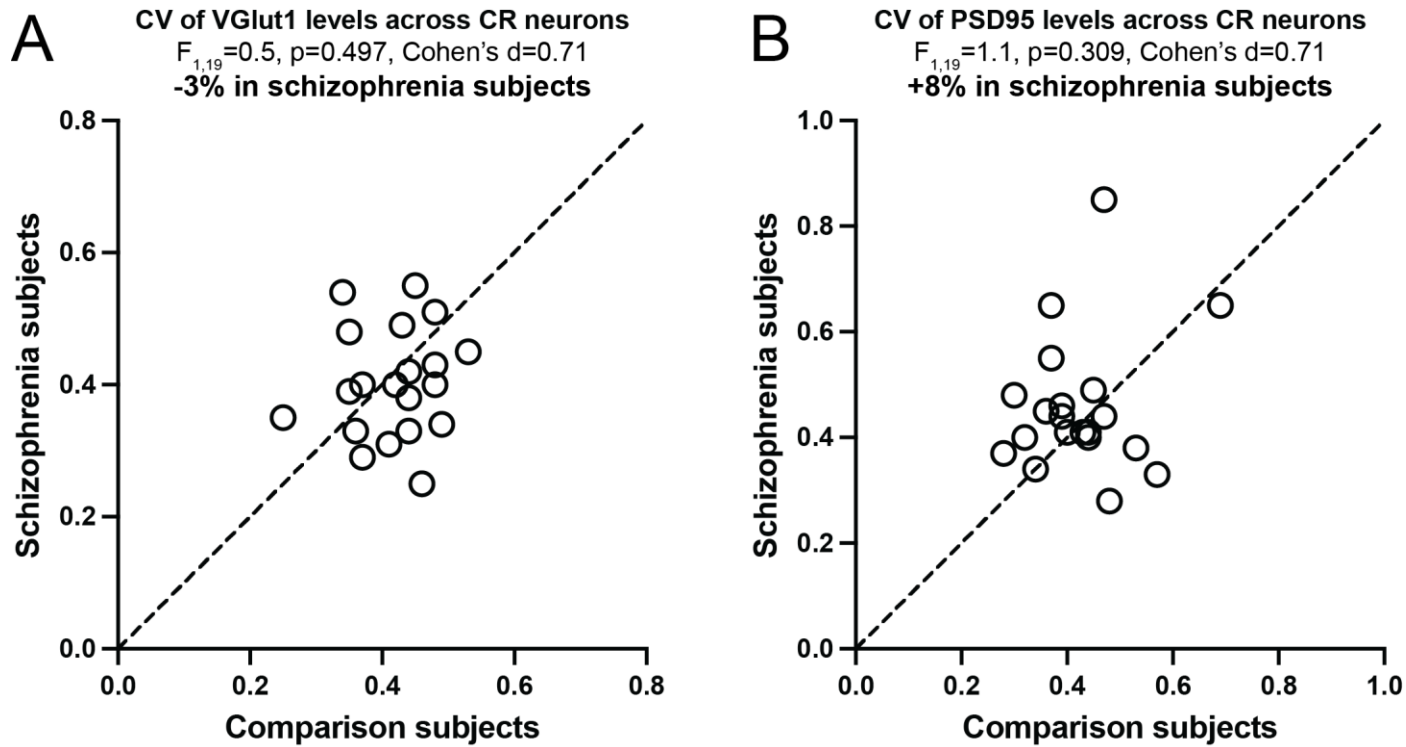

Bar graphs showing the CV of VGlut1 (A) or PSD95 (B) levels across PVIs in schizophrenia subjects grouped by presence (Yes) or absence (No) of each potential comorbid factor commonly associated with the illness. Error bars indicate standard deviation. Numbers in the bar indicate the number of schizophrenia subjects in each group. There was no significant effect of any confounding factors on the CV of VGlut1 or PSD95 levels across PV neurons in schizophrenia subjects (all p-values>0.05 after multiple comparison correction).

FIGURE S3. Lack of effect from antipsychotic medications on greater synaptic variability across PVIs
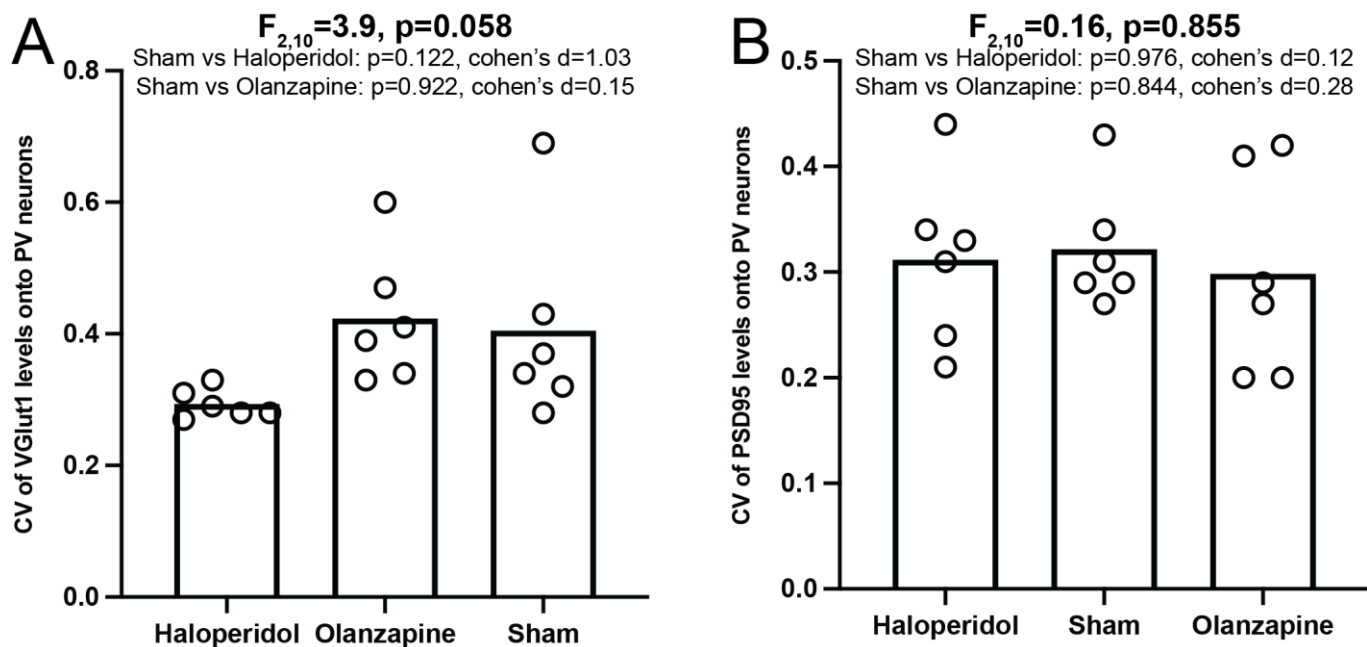

Group mean (bar) and individual monkey (open circles) levels of the CV of VGlut1 (A) or PSD95 (B) levels across PVIs in monkeys treated with haloperidol, olanzapine or sham. Statistics from post-hoc comparison and effect size analyses are shown above the graph.

FIGURE S4. Unaffected variability in excitatory synaptic strength across CR neurons in DLPFC of schizophrenia

A CV of VGlut1 levels across CR neurons
$F_{1,19}=0.5$, p=0.497, Cohen's d=0.71
-3% in schizophrenia subjects

B CV of PSD95 levels across CR neurons
$F_{1,19}=1.1$, p=0.309, Cohen's d=0.71
+8% in schizophrenia subjects

Scatterplot of CV of VGlut1(A) or PSD95 (B) levels across CR neurons for each unaffected comparison subject (x-axis) and schizophrenia subject (y-axis) in a pair. Data points above the diagonal unity line indicate a higher level in the schizophrenia subject relative to the matched unaffected comparison subject. Statistics from paired ANCOVA model and effect size analysis are shown above the graph.

FIGURE S5. Robust effect of CV_g on gamma power over background noise (σN)
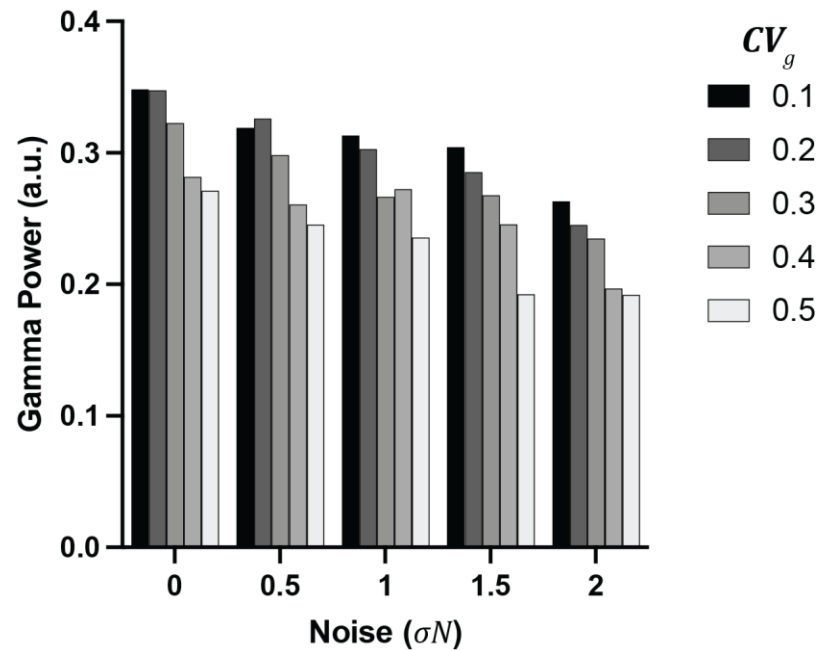
Bar graphs showing the effect of increasing CV_g from 0.1 to 0.5 on gamma power while σN increases from 0 to 2. The effect of greater CV_g on gamma power is observed over a wide range of σN.

FIGURE S6. Effect of CV_g generated from a skewed distribution on network behavior in PING model network
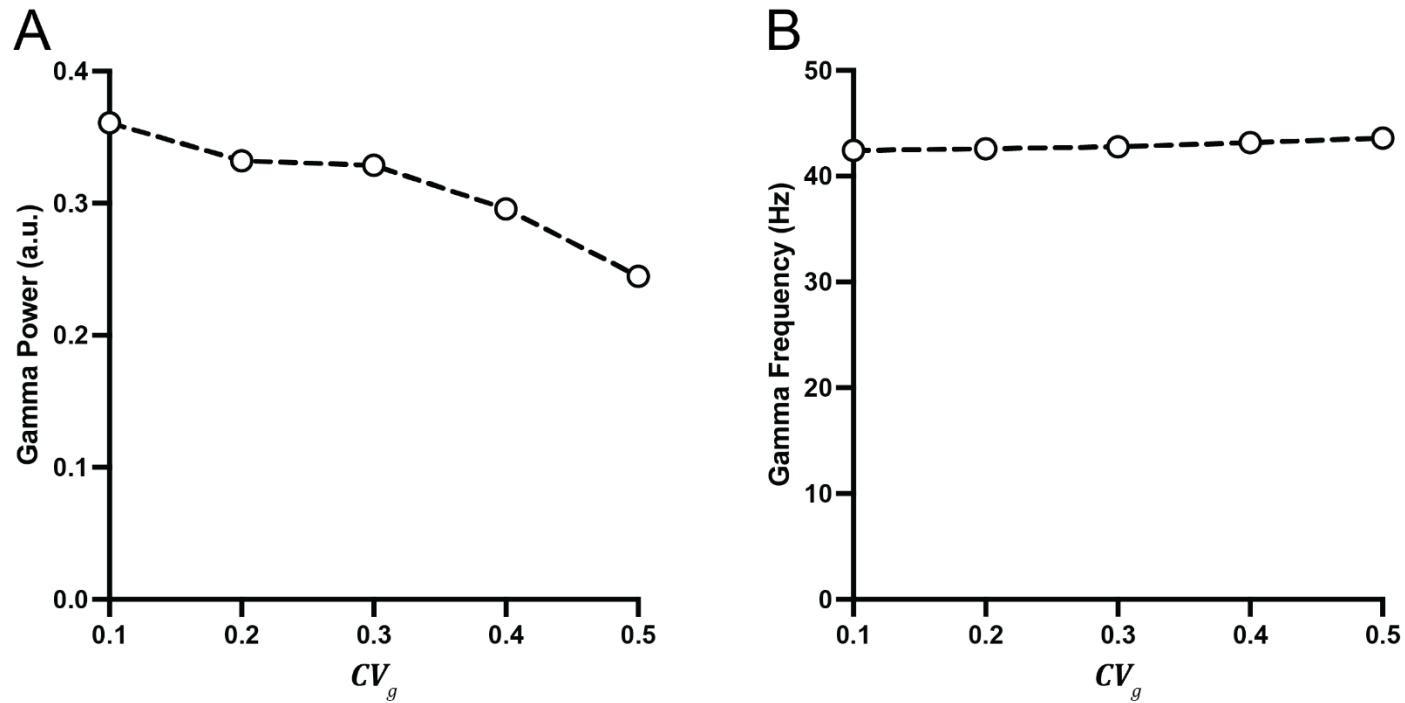
CV_g generated from a distribution with skewness of 1.58 and kurtosis of 7.57 showed magnitude of changes in peak gamma power (A) and frequency (B) similar to CV_g generated from the normal distribution, suggesting the effect of CV_g is comparable between the two distributions found in comparison and schizophrenia subject groups.

TABLE S1. Summary characteristics of study subjects from *Chung et al, 2016 (ref. 32)*

Characteristic	Unaffected comparison		Schizophrenia		
Sex	**N**	**%**	**N**	**%**	
Male	15	75	15	75	
Female	5	25	5	25	
Race	**No**	**%**	**No**	**%**	
White	16	80	14	70	
Black	4	20	6	30	
	Mean	**SD**	**Mean**	**SD**	**Paired T-test statistics**
Age (years)	46.3	12.1	45.2	11.8	$t_{19}=1.3$, p=0.209
Postmortem interval (hours)	16.4	5.5	15.4	6.3	$t_{19}=0.7$, p=0.470
Freezer storage time (months)	110.8	33.9	103.5	28.3	$t_{19}=0.9$, p=0.355

TABLE S2. The effect of diagnosis, age and sex on dependent measures from unpaired ANCOVA analyses

	CV of VGlut1 in PVIs	CV of PSD95 in PVIs	SD of VGlut1 in PVIs	SD of PSD95 in PVIs	Mean of VGlut1 in PVIs	Mean of PSD95 in PVIs	CV of VGlut1 in CR neurons	CV of PSD95 in CR neurons
Main effect of diagnosis	$F_{1,36}=6.2$, $p=0.017$	$F_{1,36}=7.9$, $p=0.008$	$F_{1,36}=4.9$, $p=0.033$	$F_{1,36}=2.2$, $p=0.142$	$F_{1,36}=0.18$, $p=0.672$	$F_{1,36}=0.15$, $p=0.697$	$F_{1,36}=0.40$, $p=0.533$	$F_{1,36}=1.2$, $p=0.281$
Effect of covariates								
Age	$F_{1,36}=0.03$, $p=0.862$	$F_{1,36}=3.2$, $p=0.083$	$F_{1,36}=0.07$, $p=0.792$	$F_{1,36}=0.75$, $p=0.393$	$F_{1,36}=0.01$, $p=0.948$	$F_{1,36}=0.09$, $p=0.764$	$F_{1,36}=0.02$, $p=0.882$	$F_{1,36}=5.2$, $p=0.029$
Sex	$F_{1,36}=0.4$, $p=0.535$	$F_{1,36}=0.4$, $p=0.544$	$F_{1,36}=0.01$, $p=0.966$	$F_{1,36}=0.13$, $p=0.723$	$F_{1,36}=0.32$, $p=0.575$	$F_{1,36}=0.22$, $p=0.644$	$F_{1,36}=0.55$, $p=0.461$	$F_{1,36}=0.39$, $p=0.536$

Supplemental References

1. Chung DW, Fish KN, Lewis DA. Pathological Basis for Deficient Excitatory Drive to Cortical Parvalbumin Interneurons in Schizophrenia. Am J Psychiatry. 2016;173:1131-1139.

2. Rotaru DC, Yoshino H, Lewis DA, Ermentrout GB, Gonzalez-Burgos G. Glutamate receptor subtypes mediating synaptic activation of prefrontal cortex neurons: relevance for schizophrenia. J Neurosci. 2011;31:142-156.

3. Gonzalez-Burgos G, Miyamae T, Pafundo DE, Yoshino H, Rotaru DC, Hoftman G, Datta D, Zhang Y, Hammond M, Sampson AR, Fish KN, Ermentrout GB, Lewis DA. Functional maturation of GABA synapses during postnatal development of the monkey dorsolateral prefrontal cortex. Cereb Cortex. 2015;25:4076-4093.

4. Hendry SH, Schwark HD, Jones EG, Yan J. Numbers and proportions of GABA-immunoreactive neurons in different areas of monkey cerebral cortex. J Neurosci. 1987;7:1503-1519.

5. Gabbott PL, Bacon SJ. Local circuit neurons in the medial prefrontal cortex (areas 24a,b,c, 25 and 32) in the monkey: II. Quantitative areal and laminar distributions. J Comp Neurol. 1996;364:609-636.

6. Izhikevich EM. Which model to use for cortical spiking neurons? IEEE Trans Neural Netw. 2004;15:1063-1070.

7. Wang XJ. Synaptic basis of cortical persistent activity: the importance of NMDA receptors to working memory. J Neurosci. 1999;19:9587-9603.